JOURNAL OF SOLID STATE CHEMISTRY **138,** 87–97 (1998)
ARTICLE NO. SC987757

A ^{57}Fe Mössbauer Study of the Cubic Perovskite-Type Phase $LaBa_2Fe_3O_{8+w}$ ($-0.20 < w < 0.83$)

J. Lindén,* M. Lippmaa,† P. Karen,‡ A. Kjekshus,‡ and M. Karppinen§

*Department of Physics, Åbo Akademi, FIN-20500 Turku, Finland; †Department of Technical Physics, Helsinki University of Technology, FIN-02150 Espoo, Finland; ‡Department of Chemistry, University of Oslo, N-0315 Oslo, Norway; and §Laboratory of Inorganic and Analytical Chemistry, Helsinki University of Technology, FIN-02150 Espoo, Finland

Received August 28, 1997; accepted January 9, 1998

Single-phase samples of $LaBa_2Fe_3O_{8+w}$ with $-0.20 \leq w \leq 0.83$ were synthesized, characterized by oxygen-content analyses, powder X-ray diffraction, and magnetic susceptibility, and investigated using ^{57}Fe Mössbauer spectroscopy. At 296 K, antiferromagnetic ordering of the Fe sites was observed for samples having $w \leq 0.45$. When $w \leq 0.0$, the iron atoms occupy predominantly an Fe^{3+}, $S = 5/2$ state, the rest being Fe^{2+}, $S = 2$. For $w \approx 0$, the intensities of the components in the Mössbauer spectra correspond to random distribution of oxygen vacancies around Fe^{3+}. When $0 \leq w \leq 0.45$, increasing amounts of iron atoms enter the Fe^{4+}, $S = 2$ state. For $w \geq 0.45$, which takes the paramagnetic state at room temperature, the amount of Fe^{4+} increases accordingly. At 85 K, there is inconclusive evidence of disproportionation of Fe^{4+} into Fe^{3+} and Fe^{5+} in the most oxidized $w = 0.83$ sample. The room-temperature Mössbauer data show that there occurs a gradual conversion from AF to P states with increasing w up to $w \geq 0.45$, when all AF components simultaneously disappear. This gradual frustration of the cooperative order has three contributing factors. First, an increasing proportion of the iron moments simply becomes paramagnetic in the AF arrangement. Second, the AF interactions become weakened upon disorder. Third, the AF interaction is obviously weakened by replacement of $S = 5/2$ with $S = 2$. The room-temperature relationship between the average internal magnetic field and the oxygen content parameter w resembles the magnetic field vs temperature relationship for a cooperative magnetic material. The common mechanism is that both temperature and oxygen loading affect the ordered spin system.

Key Words: **lanthanum barium iron oxide; perovskite-type structure oxygen content control; Mössbauer spectroscopy; magnetic properties.**

I. INTRODUCTION

Perovskite-type $ATO_{3-\delta}$ oxides of transition metals (T) have acquired a prominent position in materials science owing to properties like colossal magnetoresistance (T = Mn), high combined electronic and ionic conductivity (T = Mn, Fe, Co), and high-T_c superconductivity (T = Cu). Doping-induced structural changes in the coordination sphere of the transition metal are crucial in controlling the delicate charge balances which establish the desired properties. The superconductivity of $YBa_2Cu_3O_{6+w'}$ occurs in coincidence with a frustration of the antiferromagnetic (AF) arrangement by electron holes (1–3) which, in turn, may also be localized partially on the oxygen atoms (3–6). High electronic and ionic conductivity is observed in open (oxygen-vacant) structures doped to a nearly metallic state, which is also one of the conditions for the colossal magnetoresistance.

$LaBa_2Fe_3O_{8+w}$ is a very good mixed conductor (7) with a wide span in the oxygen content and an AF ordering at the stoichiometric composition ($w = 0$; $\mu_{AF} = 3.8\ \mu_B$), it in turn becomes frustrated on oxidation (8). The crystal structure of the phase is cubic and is related to that of the $YBa_2Fe_3O_{8+w}$ triple perovskite (9) by merging the two A-metal sites (in the present case La and Ba) and disordering of the oxygen atoms and vacancies. As a result, a homogeneity range exists with respect to the La-for-Ba substitution (10). However, the important magnetic and transport properties are largely determined by the oxygen coordinations around Fe, which, owing to the statistical nature of the disorder, are seen only as an average by diffraction methods.In this situation, Mössbauer spectroscopy is a unique tool to explore these structural details. Several Mössbauer studies (11–14) treat certain compositions of the $LaBa_2Fe_3O_{8+w}$ phase, but none deals systematically with the variable oxygen content and the Fe valence, which control the key properties.

To get an insight into structural details around the Fe atoms and observe the interplay between them and the magnetic properties, a series of $LaBa_2Fe_3O_{8+w}$ samples has been synthesized with oxygen content in the range $-0.20 < w < 0.83$. The composition data are correlated with magnetic susceptibility and Mössbauer spectroscopy measurements.

0022-4596/98 $25.00

II. EXPERIMENTAL

Syntheses. The oxides were synthesized from a precursor obtained by liquid mixing in melted citrates (15). Standardized reagent-grade components were used; dry, annealed lanthanum oxide (> 99.9%, Molycorp), dried barium carbonate (0.1% Sr, Merck), and iron lumps (99.95%, Koch-Light). The latter component was converted to nitrate by diluted HNO_3 (Baker, analyzed) prior to being added to the melted citric acid monohydrate (99%, Fluka), into which La_2O_3 had already been dissolved. $BaCO_3$ was added afterward. These citrate solutions contained approximately 4 mol of citric acid per mol of La atoms. The clear viscous melt formed by the subsequent evaporation of water was dehydrated into a solid at 180°C and incinerated at 450°C in air. The thus obtained precursor was calcined at 1000°C, pressed into tablets, and fired two to four times for a total of 500 h at 1000°C, with thorough intermediate rehomogenizations by milling in an agate vibration mill. The thus obtained master sample was subjected to sintering (1100°C for 100 h) of tablets for the oxygen-control treatments.

Oxygen content control. The equilibrium oxygen contents were controlled by the p_{O_2}, t-equilibrium with the gas atmosphere. The samples were annealed in a quenching apparatus consisting of a vertical tube furnace with the gas flow from the top and a massive brass flange with a conical hollow on the bottom, equipped with an inlet for a counterflow of dry, high-purity Ar (<1 ppm O_2). The gas outlet from the system was located between the quenching site and the furnace. The duration of the annealing was 4 to 8 days depending on temperature.

Partial pressures of oxygen above some $p_{O_2} = 10^{-4}$ atm were obtained by mixing O_2 with Ar; lower values were controlled by the high-temperature equilibrium occurring in the premixed flow of argon, hydrogen (5N purity), and water vapor. The latter was introduced from an ~42.5 wt % solution of H_3PO_4 at room temperature, and the saturated partial pressure of $p_{H_2O} \approx 0.02$ atm was corrected for the actual temperature and concentration of the H_3PO_4 solution. The high-temperature composition of the gas was calculated from the dilution ratios and the thermodynamic data (16, 17) for the H_2O formation.

Oxygen content analysis. The oxygen content of all samples was determined cerimetrically. The dissolutions of the samples in 3M HCl were carried out at some 50°C in glass ampoules sealed under Ar atmosphere. In the case of samples with Fe^{2+}, the solution was titrated directly, with ferroin as an indicator. When the sample did not contain Fe^{2+}, a specified amount of previously titrated Mohr's salt was added and the remaining excess of Fe^{2+} was determined.

Powder X-ray diffraction. The phase purity and unit-cell parameters were evaluated from powder X-ray diffraction (PXD) data obtained with a Guinier-Hägg camera with $CuK\alpha_1$ radiation and Si as an internal standard. The photographs were scanned by an LS-18 film scanner with software for X-ray data treatment (18). The threshold sensitivity toward impurities in comparable phases is tested to be better than 0.5 wt %.

Magnetic susceptibility. The magnetic susceptibility measurements were carried out in steps in the interval 5–300 K by a SQUID magnetometer (MPMS, Quantum Design) in an applied field of 50 kOe. The samples in ~50 mg lumps were contained in celluloid sample holders during the measurements.

Mössbauer spectroscopy. The Mössbauer absorbers were prepared by mixing ~80 mg of sample material with varnish and distributing it evenly on an iron-free aluminium foil. The absorber diameter was 19 mm. Room-temperature measurements in transmission geometry were performed with an Amersham ^{57}Co: Rh (20 mCi, January 1995) source. The spectra were recorded between February 1995 and April 1997. A linear velocity scale with a maximum of 15 mm/s was applied. Paramagnetic spectra were measured using a maximum velocity of 2.5 mm/s. Selected samples were also measured at 85 and 12 K in order to obtain information on the magnetic ordering. The spectra were fitted with the full Hamiltonian of combined electric and magnetic interactions. The following hyperfine parameters were thus obtained from the fits: the internal magnetic field experienced by the Fe nucleus (B), the chemical isomer shift relative to α-Fe (δ), the quadrupole coupling constant (eQV_{zz}), the resonance line widths, and the relative intensities of the components (I). The following conditions and constraints were applied: (i) For each component a certain variation in the parameter B was allowed in order to simulate the effect of local distortions of the coordination polyhedra. A Gaussian distribution was assumed and its width (ΔB) was introduced as a fit parameter, which in the actual fits was observed to vary between $\Delta B \approx 2$ T for the most reduced samples and ~5 T for the most oxidized samples. The spread in the magnetic field for a particular coordination is seen as an increase in the Mössbauer line width toward the edge of the spectrum and a leveling of the intensities compared with the ideal 3:2:1 ratio. (ii) The eQV_{zz} term gives the energy scale of the interaction between the electric field gradient (EFG) and the nuclear quadrupole moment (Q). As for B, the value of eQV_{zz} was allowed a certain spread, $\Delta(eQV_{zz})$, in the paramagnetic (P) spectra, $\Delta(eQV_{zz})$ ranging between 0.5 and 0.6 mm/s for $0.47 \leq w \leq 0.83$. In general, EFG can be expressed in terms of its main component V_{zz} and the asymmetry parameter (η), which measures the relative difference of EFG in the x and y directions. The angle θ between V_{zz} and B can either be in

the plane with or perpendicular to B, depending on the arrangement of the oxygen atoms. However, η and θ cannot be fixed in this case and these were consequently omitted as fit parameters. In fact, the contribution to η from the next-nearest neighbors should also have been considered, but such a large number of parameters was certainly not justified by the present data. Owing to these omissions, the values of eQV_{zz} are partially averaged. (iii) The *spectral* line widths of all components in a given spectrum were constrained to be equal. (iv) A small asymmetric quadrupole component, originating from traces of iron in the Be detector window, was kept fixed during the fit. This impurity defect covers less than 1% of the spectral intensity obtained in the measurements.

III. RESULTS

A. Synthesis and Characterization

After firing at 1000°C and oxygen saturation, a single-phase master sample of the composition $LaBa_2Fe_3O_{8.83}$ was obtained, with a cubic structure of the disordered perovskite type. The oxygen contents of $LaBa_2Fe_3O_{8+w}$ are variable across an appreciable span of $-0.20 < w < 0.83$ as a function of the temperature and partial pressure of oxygen ($p_{O_2} < 1$ atm) from which the samples are quenched. No sign of ordering into the $YBa_2Fe_3O_8$ triple-perovskite type is seen when the oxygen content is decreased to $w = 0$. The unit-cell parameter of the samples used for the Mössbauer measurements is plotted in Fig. 1 as a function of w.

The cubic disordered $LaBa_2Fe_3O_{8+w}$ phase equilibrates very easily in atmospheres containing oxygen. This rapid exchange of O_2 proved to be a problem when quenching from temperatures above some 1000°C was attempted for the most oxidized and most reduced compositions. The problem compositions were those with the highest mixed electronic and oxygen-ionic conductivity, which could be oxidized from the halo of gas taken up by the sample under the free fall into the quenching area (viz., within seconds before the sample is cooled to a "safe" temperature). On the reduced samples ($v_{Fe} < 3$), this procedure creates a thin brown layer (viz., trivalent iron) which slows down further oxidation. On the oxidized samples ($v_{Fe} > 3$), a relatively thick (1–2 mm) layer of an even more oxidized product is formed which hence becomes a better mixed conductor than the core itself. This black layer cannot be distinguished by eye, but has an abrupt interface with the core according to PXD; two cubic phases are seen in a mechanically homogenized sample. The oxygen contents in both the core and the surface layer are proportional to the partial pressure of oxygen and the temperature in the equilibration atmosphere. However, the mean equilibrium temperature experienced by the core and the surface layer is different. In order to avoid the reoxidation problem, the surface layer was removed, and quenching from below 900°C was adopted for the oxidized samples. With these simple precautions, no admixture of the more oxidized composition was observed by PXD in the homogenized samples used for the property measurements.

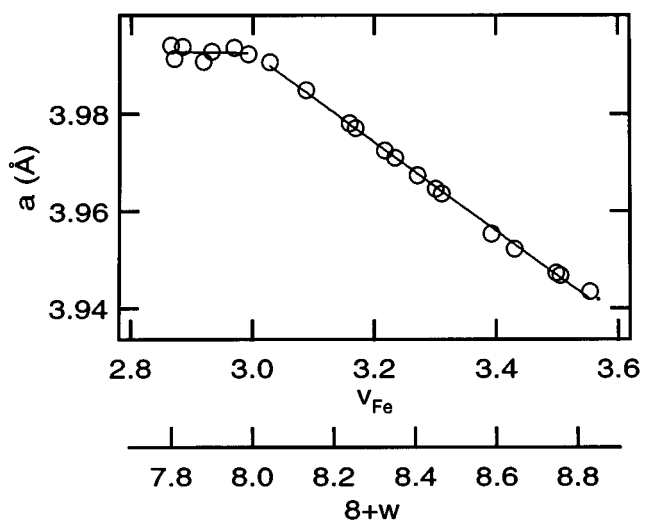

FIG. 1. Perovskite-type unit-cell parameter a as a function of average Fe valence (v_{Fe}) and oxygen content ($8 + w$) for $LaBa_2Fe_3O_{8+w}$. Estimated errors do not exceed the size of symbol.

Another chemically related experimental problem was encountered in that the samples containing Fe^{2+} oxidized slowly at room temperature, even by the traces of O_2 left after flushing the storage containers by Ar. As a result, the oxygen content increased by some 0.02–0.05 in the period (less than a month) between the synthesis and the collection of the Mössbauer spectra.

The temperature and partial pressure of oxygen from which the samples used for the Mössbauer spectroscopic measurements were quenched are shown in Fig. 2. In order to provide a *phenomenological* description, isotherms are drawn based on a least-squares fitting according to a simplified model with chemical point-defect equilibria. For this purpose, $LaBa_2Fe_3O_{8+w}$ is considered an acceptor-doped $LaFeO_3$ compensated by oxygen vacancies (oxygen interstitials are neglected). The oxygen exchange proceeds according to:

$$O_2 + 2V_O^{\bullet\bullet} \rightleftharpoons 4h^{\bullet} + 2O_O^{\times} \qquad [1]$$

and

$$2O_O^{\times} \rightleftharpoons 4e' + 2V_O^{\bullet\bullet} + O_2 \qquad [2]$$

for iron oxidation states above and below $+3$, respectively. The concentration of the oxygen vacancies as a function of the partial pressure of oxygen is expressed by combination

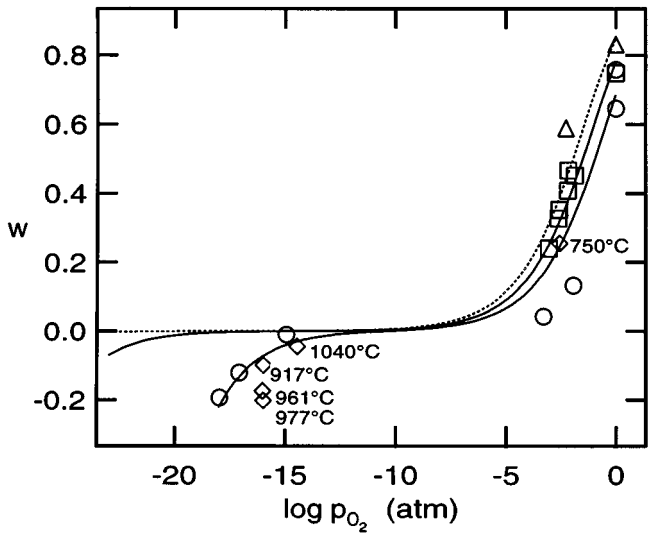

FIG. 2. Quenching conditions (t, pO_2) for $LaBa_2Fe_3O_{8+w}$ samples used for Mössbauer measurements (○: $t = 900°C$, □: $t = 600°C$, △: $t = 450°C$, and ◇: as specified on the illustration). Curves indicate fitted isotherms for 900, 600, and 450°C, the latter dotted.

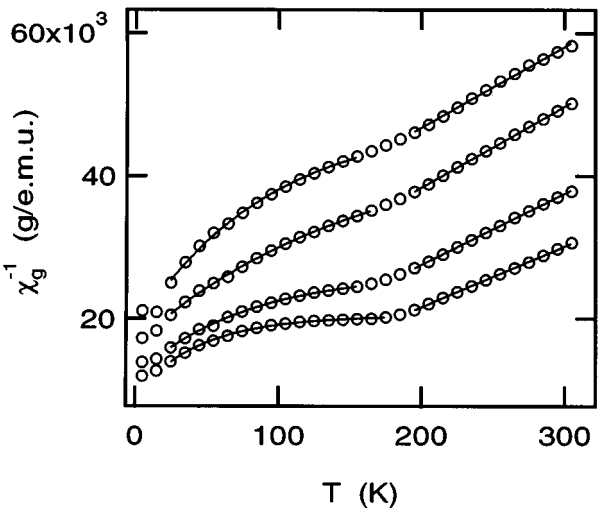

FIG. 3. Reciprocal magnetic susceptibilities for oxidized $LaBa_2Fe_3O_{8+w}$. From top (quenching temperatures in °C): $w = 0.60$ (900), 0.65 (450), 0.76 (900), 0.83 (450). Lines and curves as fitted to evaluate T_N and μ_P (Table 1).

of the equilibrium constants for Eqs. [1] and [2] and the electroneutrality condition $[e'] + [Ba'_{La}] = [h^\bullet] + 2[V_O^{\bullet\bullet}]$. The temperature dependences of the equilibrium constants are introduced via van't Hoff expressions. The solution of the resulting polynomial, in the form of $\log[V_O^{\bullet\bullet}]$ as a function of $\log p_{O_2}$ and temperature, is fitted to the experimental data, and the result is replotted in terms of the compositional parameter w in Fig. 2. It can be seen that the w values obtained under quenching are reasonably consistent in that no major violations of the expected trends in p_{O_2} and temperature occur.

B. Magnetic Susceptibility

According to powder neutron diffraction (PND), the magnetic moments in $LaBa_2Fe_3O_{8+w}$ order antiferromagnetically, with Néel temperatures (T_N) around 650 K when $v_{Fe} \approx 3.0$, decreasing to around 185 K for highly oxidized samples (8). The (reciprocal) magnetic susceptibilities of several such high-oxygen single-phase samples are plotted in Fig. 3, and it is seen that T_N is practically independent of the oxygen content. This indicates that there is a constant structural component governing the magnetic properties of highly oxidized $LaBa_2Fe_3O_{8+w}$, possibly corresponding to one of the orderings seen by HREM in Ref. (19) for $NdBa_2Fe_3O_{8+w}$. The P moments μ_P evaluated from the data in Fig. 3 and the spin quantum numbers S_P calculated on the assumption of quenched orbital contribution (spin-only approximation) are listed in Table 1. Somewhat surprisingly, the P moment appears to diminish in the direction toward the trivalent Fe state.

C. Mössbauer Spectroscopy

Room-temperature spectra and fitted curves for selected $LaBa_2Fe_3O_{8+w}$ compositions w are shown in Fig. 4. The general feature is that the distinct AF components present at low values of w broaden and decrease appreciably shortly before they vanish close to $w = 0.45$ on a gradual increase of P components. For $w = 0.47$, a pure P spectrum appears at room temperature, whereas AF order is still present at 85 K (Fig. 5). The simultaneous disappearance of all the magnetic components as a function of w also confirms that the measured samples are compositionally homogeneous.

Altogether, five AF components have been identified in the spectra. Three of them dominate for low values of $|w|$ and were assigned to trivalent iron with spin state $S = 5/2$ situated in structural environments specified by the coordination numbers (CN): Octahedral, designated with the composite notation ${}^{CN6}_{AF}Fe^{3+}_{S5/2}$; square-pyramidal, with notation ${}^{CN5}_{AF}Fe^{3+}_{S5/2}$; and tetrahedral, with notation ${}^{CN4}_{AF}Fe^{3+}_{S5/2}$

TABLE 1

Néel Temperatures (K), P Moments μ_P (μ_B), and Spin Quantum Numbers S_P of Fe, Extracted for the Highly Oxidized $LaBa_2Fe_3O_{8+w}$ Samples from Fig. 3

w	T_N	μ_P	S_P
0.60	170	4.11(2)	1.61
0.65	178	4.11(2)	1.62
0.76	174	4.39(2)	1.75
0.83	184	4.75(2)	1.93

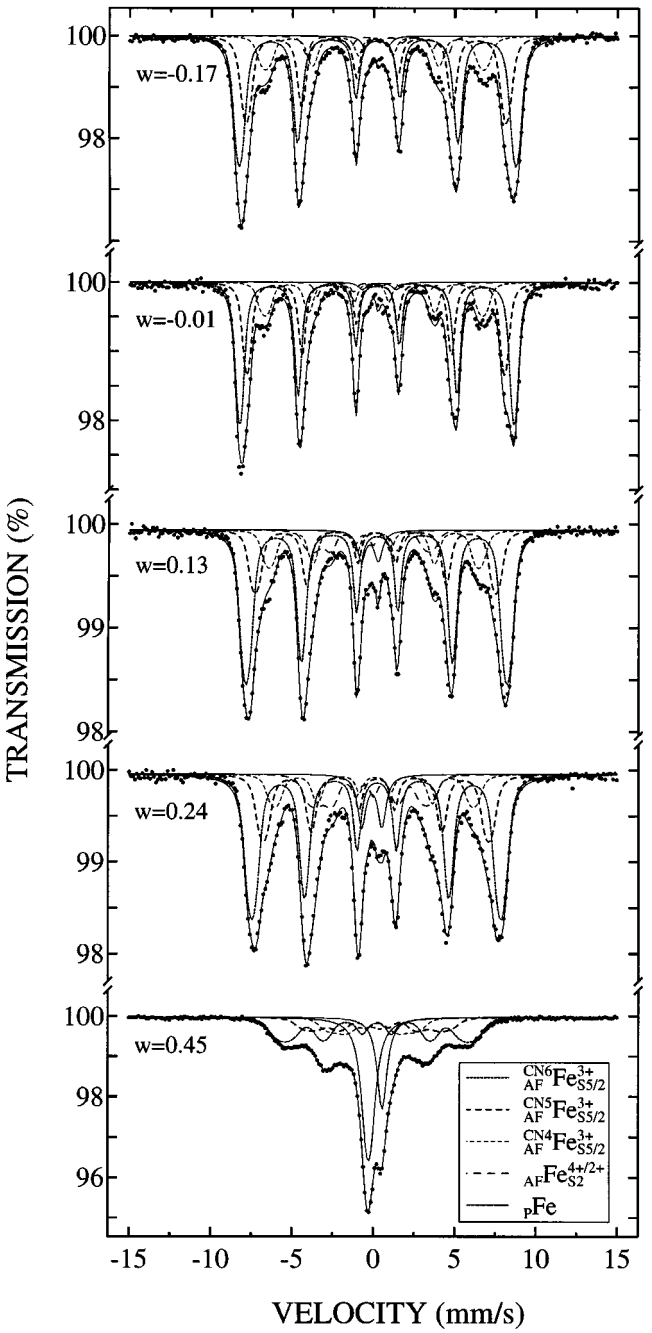

FIG. 4. Mössbauer spectra of $LaBa_2Fe_3O_{8+w}$ at 296 K. Labeling of the components is shown at the bottom of the illustration.

(listed in decreasing order of spectral intensity.) The two remaining components were assigned to $_{AF}Fe^{2+}_{S2}$ and $_{AF}Fe^{4+}_{S2}$, and their intensities vary with w.

In all AF spectra, a general paramagnetic component designated $_{P}Fe$ is present, with intensity increasing from some 1–2% for $w \leq 0$ to around 40% just before the disappearance of the AF state at room temperature (Fig. 4,

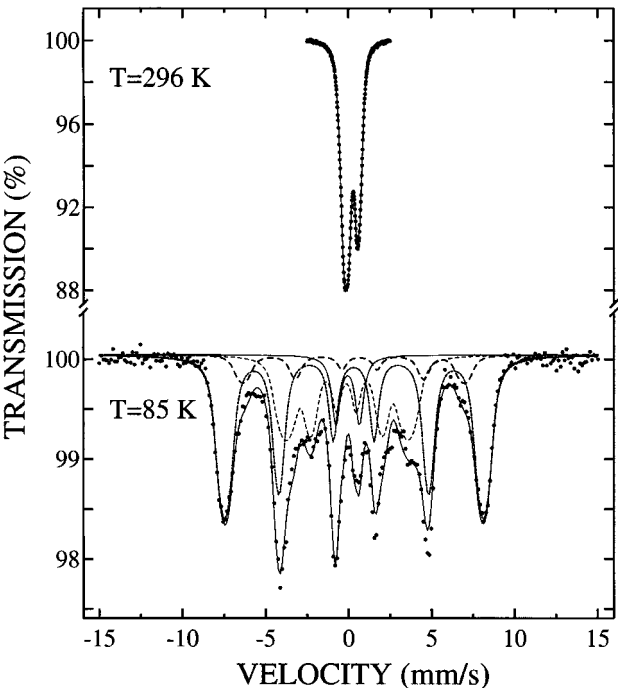

FIG. 5. Mössbauer spectra of $LaBa_2Fe_3O_{8.47}$ recorded at 296 and 85 K. For labeling of the AF components, see Fig. 4.

$w = 0.45$, and *vide infra*). This $_{P}Fe$ component then changes smoothly into the characteristic double-peak feature of the paramagnetic spectra for higher values of the oxygen content parameter w. Only for the most oxidized sample with predominantly CN6 could this general $_{P}Fe$ component be unambiguously separated into two subcomponents with specific valence states $_{P}Fe^{3+}$ and $_{P}Fe^{4+}$.

1. AF Component Assignments

The hyperfine parameters (with calculated standard deviations) of the AF components, derived from the 296 K Mössbauer spectra are presented in Table 2, and low-temperature values are given in Table 3.

Internal fields. The internal magnetic field depends on three factors: the spin density at the Mössbauer nucleus (the Fermi contact term), the orbital term, and the dipolar term (20). The last term is small for an antiferromagnetic substance, but the two former can be of equal magnitude and opposite sign. The internal magnetic fields may also contain supertransferred hyperfine fields from the nearest-neighbor spins, which can result in multiple hyperfine fields from different coordinates. The largest components, designated $^{CN6}_{AF}Fe^{3+}_{S5/2}$ and $^{CN5}_{AF}Fe^{3+}_{S5/2}$, have internal fields close to 50 T at room temperature. This is conceivable only for the high-spin, trivalent iron state, for which the orbital term of the

TABLE 2
Internal Magnetic Fields (B), Chemical Isomer Shifts (δ), Quadrupole Coupling Constants (eQV_{zz}), and Spectral Intensities (I) for AF components of Mössbauer Spectra of $LaBa_2Fe_3O_{8+w}$ at 296 K

	B (T)					δ (mm/s)				
w	${}^{CN6}_{AF}Fe^{3+}_{S5/2}$	${}^{CN5}_{AF}Fe^{3+}_{S5/2}$	${}^{CN4}_{AF}Fe^{3+}_{S5/2}$	${}_{AF}Fe^{2+}_{S2}$	${}_{AF}Fe^{4+}_{S2}$	${}^{CN6}_{AF}Fe^{3+}_{S5/2}$	${}^{CN5}_{AF}Fe^{3+}_{S5/2}$	${}^{CN4}_{AF}Fe^{3+}_{S5/2}$	${}_{AF}Fe^{2+}_{S2}$	${}_{AF}Fe^{4+}_{S2}$
−0.20	52.74(3)	49.56(5)	41.58(7)	27.02(6)		0.353(2)	0.291(3)	0.182(6)	0.729(8)	
−0.19	52.45(6)	49.3(1)	42.4(3)	26.6(2)		0.345(4)	0.292(6)	0.19(2)	0.72(2)	
−0.17	52.85(5)	49.67(7)	41.68(9)	26.99(9)		0.355(3)	0.286(4)	0.19(1)	0.74(1)	
−0.12	51.91(4)	48.85(6)	41.0(1)	26.5(1)		0.344(3)	0.284(5)	0.11(2)	0.73(3)	
−0.10	52.85(5)	49.87(7)	41.93(5)	24.94(8)		0.352(2)	0.275(4)	0.073(6)	0.90(1)	
−0.05	53.16(7)	50.4(1)	42.04(7)	25.23(1)		0.365(5)	0.271(5)	0.052(7)	0.90(1)	
−0.01	52.29(4)	49.10(6)	41.5(1)	24.7(2)		0.350(3)	0.290(5)	0.07(1)	0.92(3)	
0.04	51.63(4)	48.53(7)	41.37(6)		24.9(1)	0.342(2)	0.275(3)	0.042(6)		−0.03(1)
0.13	49.7(1)	45.9(4)	40.0(2)		22.4(3)	0.330(3)	0.276(8)	0.14(2)		−0.28(3)
0.24	47.4(1)	42.9(3)	37.9(3)		21.6(2)	0.330(3)	0.311(7)	0.20(2)		−0.25(2)
0.25	46.2(1)	41.3(5)	36.2(4)		20.4(1)	0.322(3)	0.290(8)	0.25(2)		−0.25(2)
0.33	43.48(9)	36.0(2)			19.1(2)	0.308(4)	0.26(1)			−0.26(2)
0.35	41.2(1)	33.0(3)			17.7(3)	0.290(5)	0.27(2)			−0.27(1)
0.41	37.8(1)	28.8(3)			16.9(2)	0.32(1)	0.41(2)			−0.03(2)
0.45	35.1(2)	25.4(6)			15.9(4)	0.33(1)	0.39(2)			0.11(3)

	eQV_{zz} (mm/s)					I (%)[a]				
w	${}^{CN6}_{AF}Fe^{3+}_{S5/2}$	${}^{CN5}_{AF}Fe^{3+}_{S5/2}$	${}^{CN4}_{AF}Fe^{3+}_{S5/2}$	${}_{AF}Fe^{2+}_{S2}$	${}_{AF}Fe^{4+}_{S2}$	${}^{CN6}_{AF}Fe^{3+}_{S5/2}$	${}^{CN5}_{AF}Fe^{3+}_{S5/2}$	${}^{CN4}_{AF}Fe^{3+}_{S5/2}$	${}_{AF}Fe^{2+}_{S2}$	${}_{AF}Fe^{4+}_{S2}$
−0.20	−0.005(6)	−0.128(9)	−0.20(3)	−1.70(3)		48(1)	31(1)	16(1)	5.1(2)	
−0.19	0.04(2)	−0.19(2)	−0.35(8)	−1.69(9)		45(1)	33(1)	16(1)	4.2(4)	
−0.17	−0.028(9)	−0.11(1)	−0.13(4)	−1.73(5)		47(1)	31(1)	15(1)	4.9(3)	
−0.12	−0.016(7)	−0.07(1)	−0.13(4)	−1.76(4)		46(1)	34(1)	14(1)	4.5(2)	
−0.10	−0.054(7)	−0.12(1)	0.19(2)	−0.97(4)		48(1)	31(1)	15(1)	4.5(2)	
−0.05	−0.030(9)	−0.06(1)	0.29(3)	−1.13(6)		46(2)	35(2)	14(1)	3.8(2)	
−0.01	−0.06(1)	−0.11(2)	0.26(5)	−1.1(1)		48(1)	31(1)	15(1)	3.7(4)	
0.04	−0.047(6)	−0.10(6)	0.37(2)		2.09(5)	48(1)	27(1)	17(1)		5.1(2)
0.13	−0.022(9)	−0.09(3)	0.05(6)		0.8(1)	51(1)	21(2)	14(1)		8.7(3)
0.24	−0.03(1)	−0.06(3)	−0.11(6)		0.64(7)	48(2)	22(1)	11(1)		13(1)
0.25	−0.01(1)	−0.08(3)	−0.37(9)		0.31(4)	47(2)	22(1)	9(2)		15(1)
0.33	0.01(1)	−0.37(6)			0.14(4)	55(2)	20(1)			17(1)
0.35	0.00(2)	−0.67(7)			0.05(6)	55(1)	17(1)			18(1)
0.41	−0.01(4)	−0.50(5)			−0.11(5)	45(2)	19(2)			19(1)
0.45	−0.05(5)	−0.14(7)			0.02(6)	30(1)	16(1)			14(1)

[a] Rounded-off intensities, the rest to 100% is ${}_{P}Fe$.

internal magnetic field is zero. The ${}^{CN4}_{AF}Fe^{3+}_{S5/2}$ component has a maximum field around 42 T, which may still correspond to the high-spin state, whereas ${}_{AF}Fe^{2+}_{S2}$ and ${}_{AF}Fe^{4+}_{S2}$ have maximum fields of some 25 T. This lends some support to the assigned spin state $S = 2$, which, however, cannot be based solely on the internal field value since both the contact and orbital terms are nonzero. When the AF state is about to disappear as a function of w, B decreases rapidly and this causes broadening which in the fits was taken care of by the distribution parameter ΔB.

Isomer shifts. The isomer-shift parameter δ measures mainly the s electron density at the nucleus, and can be used to determine the valence and spin state of the Fe atoms. A list of possible isomer shift values for iron in various valence and spin states is presented in Table 4. The components ${}^{CN6}_{AF}Fe^{3+}_{S5/2}$ and ${}^{CN5}_{AF}Fe^{3+}_{S5/2}$ have δ between 0.26 and 0.36 mm/s, which fits all the spin states of trivalent, but none of tetravalent iron (it is the high value of the internal magnetic field which speaks for the high-spin assignment). The isomer shift of the component ${}^{CN4}_{AF}Fe^{3+}_{S5/2}$ is lower (0.04–0.25 mm/s), and this means that it could also correspond to $Fe^{3+}_{S1/2}$, if it were not for the relatively high value of the internal field. Another candidate, Fe^{4+}_{S2}, is excluded for chemical reasons, since this component occurs across the entire composition span in w. The discrepancy in the actual value of δ can be attributed to the fact that the resonance lines of the ${}^{CN4}_{AF}Fe^{3+}_{S5/2}$ component are overlapping with the

TABLE 3
Mössbauer Hyperfine Parameters for $LaBa_2Fe_3O_{8+w}$ at 85 K

	B (T)					δ (mm/s)				
w	$^{CN6}_{AF}Fe^{3+}_{S5/2}$	$^{CN5}_{AF}Fe^{3+}_{S5/2}$	$^{CN4}_{AF}Fe^{3+}_{S5/2}$	$_{AF}Fe^{2+}_{S2}$	$_{AF}Fe^{4+}_{S2}$	$^{CN6}_{AF}Fe^{3+}_{S5/2}$	$^{CN5}_{AF}Fe^{3+}_{S5/2}$	$^{CN4}_{AF}Fe^{3+}_{S5/2}$	$_{AF}Fe^{2+}_{S2}$	$_{AF}Fe^{4+}_{S2}$
− 0.01	54.99(6)	54.1(1)	46.0(2)	27.2(3)		0.53(1)	0.25(2)	0.17(2)	0.96(5)	
0.33	52.6(1)	49.1(4)	43.4(4)		24.9(4)	0.424(4)	0.39(2)	0.56(3)		0.03(3)
0.45	50.79(7)	46.3(2)			24.3(2)	0.412(4)	0.43(1)			− 0.03(3)
0.47	48.27(6)	41.3(6)			23.0(2)	0.419(5)	0.58(4)			− 0.01(2)
0.65	45.5(1)	36.9(7)			21.4(2)	0.41(1)	0.79(7)			− 0.06(2)
0.83	46.3(1)	41.6(4)			24.70(8)	0.397(7)	0.48(3)			0.03(1)
0.83[a]	49.1(2)	44.2(7)			27.5(3)	0.38(3)	0.3(1)			0.01(4)
	eQV_{zz} (mm/s)					I (%)[b]				
w	$^{CN6}_{AF}Fe^{3+}_{S5/2}$	$^{CN5}_{AF}Fe^{3+}_{S5/2}$	$^{CN4}_{AF}Fe^{3+}_{S5/2}$	$_{AF}Fe^{2+}_{S2}$	$_{AF}Fe^{4+}_{S2}$	$^{CN6}_{AF}Fe^{3+}_{S5/2}$	$^{CN5}_{AF}Fe^{3+}_{S5/2}$	$^{CN4}_{AF}Fe^{3+}_{S5/2}$	$_{AF}Fe^{2+}_{S2}$	$_{AF}Fe^{4+}_{S2}$
− 0.01	0.02(2)	− 0.21(3)	0.13(6)	− 1.1(2)		46(3)	33(3)	17(2)	3(1)	
0.33	− 0.04(1)	− 0.17(5)	− 1.2(1)		− 0.17(2)	53(4)	18(3)	9(1)		15(1)
0.45	0.00(2)	− 0.19(6)			0.25(6)	52(2)	16(2)			26(1)
0.47	0.05(2)	− 0.7(1)			0.07(5)	53(4)	9(1)			31(1)
0.65	0.13(5)	− 0.9(2)			0.12(7)	40(3)	10(2)			40(1)
0.83	0.00(3)	− 0.3(1)			− 0.02(4)	41(3)	11(2)			41(1)
0.83[a]	0.0(1)	0.4(4)			− 0.1(2)	51(4)	8(3)			41(3)

[a] Measured at 12 K.
[b] Rounded-off intensities, the rest to 100% is $_{P}Fe$.

dominating components $^{CN6}_{AF}Fe^{3+}_{S5/2}$ and $^{CN5}_{AF}Fe^{3+}_{S5/2}$. The δ values for $_{AF}Fe^{2+}_{S2}$ are between 0.72 and 0.92 mm/s, clearly supporting the assignment. The assigned $_{AF}Fe^{4+}_{S2}$ component has δ between − 0.28 and − 0.03 mm/s, and the only candidates in this range of δ which exhibit magnetic splitting are $Fe^{3+}_{S1/2}$ and Fe^{4+}_{S2}. The former is a less likely alternative based on the value of the internal field and the relative intensity.

Note that reasonably reliable comparisons of experimental isomer shifts with literature values are only meaningful for $w < 0.4$ owing to the large line broadening close to crossover between AF and P state at room temperature.

TABLE 4
Possible Isomer Shift Values for Various Valence and Spin States of Fe According to Ref. (21)

State	Min δ (mm/s)	Max δ (mm/s)
$Fe^{5+}_{S3/2}$[a]	− 0.13	0.10
Fe^{4+}_{S2}	− 0.14	0.14
Fe^{4+}_{S1}	0.11	0.24
$Fe^{3+}_{S5/2}$	0.19	0.54
$Fe^{3+}_{S3/2}$	0.23	0.36
$Fe^{3+}_{S1/2}$	− 0.17	0.40
Fe^{2+}_{S0}	− 0.27	0.40
Fe^{2+}_{S1}	0.27	0.50
Fe^{2+}_{S2}	0.77	1.50

[a] Ref. (12).

Quadrupole coupling constants. The quadrupole coupling has two sources: the surrounding lattice ions and the valence electrons of the Mössbauer probe. If, however, the valence shell is exactly half full, the latter contribution amounts to zero, since the valence electron density is spherically distributed (22) (making the orbital term of the magnetic field zero as well). This is precisely the case for the $Fe^{3+}_{S5/2}$ state. Therefore its eQV_{zz} should depend only on the lattice contribution, which has its origin mainly in the oxygen coordination.

A symmetrical octahedral oxygen surrounding gives zero contribution to eQV_{zz}, and this is consistent with the assignment of the $^{CN6}_{AF}Fe^{3+}_{S5/2}$ component. A square-pyramidal oxygen coordination gives a small contribution to eQV_{zz}, as seen for the component $^{CN5}_{AF}Fe^{3+}_{S5/2}$. The $^{CN4}_{AF}Fe^{3+}_{S5/2}$ component has a substantial eQV_{zz}, and this is consistent with four-coordinated iron in square-planar and deformed tetrahedral coordinations.

Intensities. Generally for an oxygen-vacant, disordered cubic perovskite-type structure, an assumption of a random oxygen distribution over all available oxygen sites can be adopted. According to this assumption, approximately 98% of the intensity in the Mössbauer spectra of stoichiometric $LaBa_2Fe_3O_{8.00}$ should refer to components originating at

sites with CN6, CN5, and CN4 of Fe. By assuming a random (binomial) distribution of the oxygen atoms, the probability for a specific oxygen position (of the 3*c* site in $Pm\bar{3}m$) being occupied is 8/9 (for $w = 0$). Thus the probability for having a six-coordinated Fe atom is $(\frac{8}{9})^6 \approx 0.49$. The coordination number five has the probability $\binom{6}{1}(\frac{8}{9})^5(\frac{1}{9}) \approx 0.37$, while four-coordinated Fe is obtained with a probability of $\binom{6}{2}(\frac{8}{9})^4(\frac{1}{9})^2 \approx 0.12$ (12). Other coordinations should occur with a total probability of less than 0.02. These predictions agree very well with the distribution of these coordinations according to the experimental intensities for $w \approx 0$, which in corresponding figures give 0.48, 0.31, and 0.16 for also six-, five- and four-coordinated trivalent iron, respectively. When *w* increases, the random oxygen model also predicts the observed disappearance of the four-coordinated site and the decrease of the five-coordinated site.

The intensity of the component ${}_{AF}Fe_{S2}^{2+}$ (assigned for the samples with $w < 0$) increases less than expected with decreasing *w*, and this may in part be caused by the tendency of the most heavily reduced samples to oxidize (see note added in proof). However, due to overlap, the ${}_{AF}Fe_{S2}^{2+}$ intensities strongly correlate with intensities of the other, dominating components. The assignment of this component is hence based mainly on the value of the isomer shift.

The intensity of the ${}_{AF}Fe_{S2}^{4+}$ component follows the amount of Fe^{4+} balanced from the compositions according to $\frac{2}{3}w \cdot 100$ (%; Tables 2 and 3). Figure 6 shows the average valence of Fe, derived from the *identified* AF and P components in the Mössbauer spectra (the consequences of possible differences in the valence of the nonresolved ${}_{P}Fe$ components being neglected). In the literature, a disproportionation of Fe^{4+} into Fe^{3+} and Fe^{5+} has been reported for related highly oxygenated phases (23–26). The $LaBa_2Fe_3O_{8+w}$ samples which could exhibit this feature are paramagnetic at room temperature, but become AF-ordered at low temperatures, and this improves the resolution of the Mössbauer components. The intensity of the ${}_{AF}Fe_{S2}^{4+}$ component at 85 K (Table 3) follows very closely the expected percentage of Fe^{4+} up to $w = 0.65$. Only for the most oxidized sample ($w = 0.83$) measured at 12 K could a partial disproportionation of Fe^{4+} into Fe^{3+} and Fe^{5+} be considered feasible in order to match the intensity of this component with *w*. This is in line with Mössbauer studies (25, 27) on similar oxides with formally tetravalent iron which suggest that the charge disproportionation of Fe^{4+} occurs gradually with composition and is hence not necessarily complete. Additional evidence may come from the increase in the internal field for $w = 0.83$ (at 85 K) compared with $w = 0.65$ (Table 3).

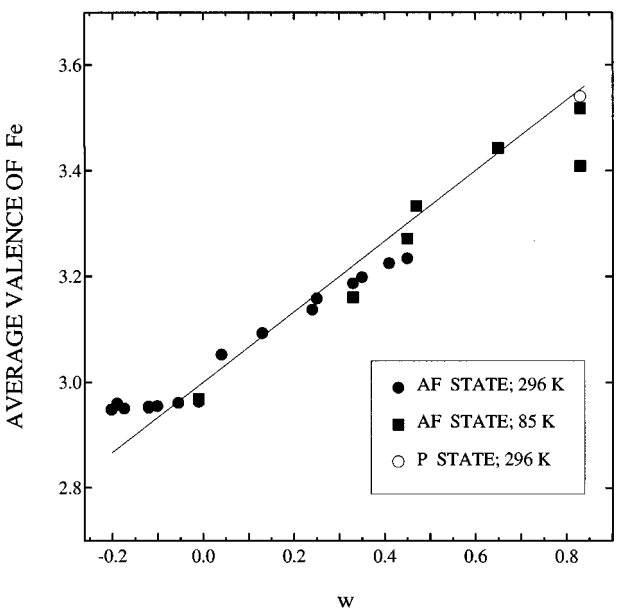

FIG. 6. Average valence of iron in $LaBa_2Fe_3O_{8+w}$. Mössbauer data are shown by points (identified in the legend); the solid line gives the theoretical prediction according to the composition parameter *w*.

2. *P Component Assignments*

The general ${}_{P}Fe$ component identified in the spectra of the AF samples could not be further separated into individual iron states. Neither is the resolution unique in the pure P spectra with quadrupolar interaction only. Good fits could be obtained with components having either large eQV_{zz} and fairly equal values for δ, or small eQV_{zz} and differing values for δ. In order to maintain comparable eQV_{zz} for both AF and P states, the latter alternative was chosen. A further reason for this choice was that an increase *w* necessarily increases the proportion of CN6 in the cubic perovskite-type structure, and this coordination is not conceivable with large quadrupole coupling constants.

Of the samples which are paramagnetic at room temperature, only the most oxidized, $w = 0.83$, sample could be well fitted with two components (see also Refs. (12, 27)). Based on the isomer shift values, these components have been assigned as ${}_{P}Fe^{3+}$ and ${}_{P}Fe^{4+}$. This assignment also fits well into the overall picture of the average, Mössbauer-based valence of Fe in Fig. 6. According to structural considerations, these two states occupy mostly CN6. The refined parameters for the $w = 0.83$ sample are listed in Table 5.

TABLE 5
Mössbauer Hyperfine Parameters for P Components in $LaBa_2Fe_3O_{8.83}$ at 296 K

Component	δ (mm/s)	eQV_{zz} (mm/s)	*I* (%)
${}_{P}Fe^{3+}$	0.369(5)	0.29(2)	46(1)
${}_{P}Fe^{4+}$	0.023(4)	0.29(2)	54(1)

In the spectra of the samples with oxygen content lower than $w = 0.83$, at least one additional P component appears. The peak which originates from the Fe^{4+} peak for $w = 0.83$ is broadened and can be fitted with two or perhaps even more components. Unfortunately, these heavily overlapped components cannot be separated sufficiently (Fig. 7), even when only two such contributions are considered. Since these additional P components occur on oxygen depletion of a perovskite-type structure, a reasonable inference may be that they represent Fe^{3+} in less than six coordination.

IV. DISCUSSION

The wide homogeneity region of the $LaBa_2Fe_3O_{8+w}$ phase makes it an excellent example of a system with high concentrations of electron ($w < 0$) and hole ($w > 0$) charge carriers in interaction with a long-range magnetic order. Although as an electron carrier the phase is rather uninteresting, the increasingly high hole concentrations which occur on oxygen loading ($w > 0$) seem to be associated with a gradual frustration of the magnetic order. The frustration has two (or really three) aspects: (i) An increasing portion of the iron moments becomes paramagnetic next to the still-prevailing AF order. This is manifested in the Mössbauer intensities of the P and AF components. (ii) The AF interactions become weakened, the moments increasingly "oscillate" around their ideal ordered directions, and this is manifested in a gradual decrease in the internal magnetic field of the AF components. This process hence leads to an increase in the reduced temperature T/T_N on increasing w for data collected at a fixed temperature. (Note that the AF interaction obviously is also weakened by the replacement of $S = 5/2$ with $S = 2$ as w increases.)

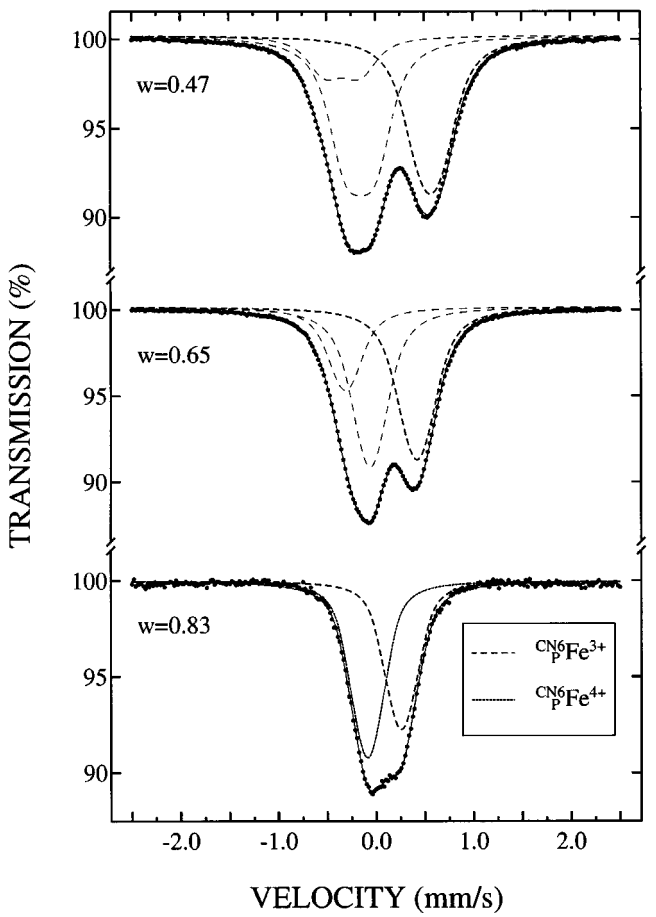

FIG. 7. Mössbauer spectra at 296 K of oxidized $LaBa_2Fe_3O_{8+w}$ samples. Identified components are labeled. Examples of fits for the poorly resolved unidentified components in the samples with $w = 0.47$ and 0.65 are shown by thin large-spaced dashed lines.

Both these processes have a common cause, the oxygen loading. This is of a local nature, as is the formation of the associated P centers. On the other hand, the weakening of the AF state is apparently more homogeneous, resembling the effect of increasing temperature. Since the oxygen loading increases the bond valence locally, it is expected that the P centers should contain more of the oxidized Fe state, viz., Fe^{4+}. This indeed seems to be the case, judging from the apparent depletion of the ${}_{AF}Fe_{S2}^{4+}$ state just before the AF order disappears as a function of w at 296 K (see, e.g., the data for $w = 0.45$ in Table 2).

In the following, the variation in the observed Mössbauer intensities and internal fields with w will be considered in more detail with respect to the two aspects of the frustration of the AF order. In Fig. 8, two average fractional Mössbauer parameters associated with the two mechanisms are plotted as a function of w. The parameter x_{AF} expresses the (mole) fraction of the AF-ordered iron sites ($x_P = 1 - x_{AF}$ is the fraction of the P sites), based on the Mössbauer intensities of the individual AF components i:

$$x_{AF} = \sum_i \frac{I_{i,w}}{100} \qquad [3]$$

The parameter ξ_B^{AF} is designed to reflect the relative value of the average B at the AF sites:

$$\xi_B^{AF} = \sum_i \left(\frac{B_{i,w}}{B_{i,w=0}} \cdot \frac{I_{i,w}}{\sum_i I_{i,w}} \right). \qquad [4]$$

Only room-temperature data are used in Fig. 8 for consistency reasons. The product of x_{AF} and ξ_B^{AF},

$$x_{AF} \cdot \xi_B^{AF} = \sum_i \left(\frac{B_{i,w}}{B_{i,w=0}} \cdot \frac{I_{i,w}}{100} \right), \qquad [5]$$

in turn reflects the relative value of the average B across the sample as a whole. The inset to Fig. 8 shows the relative contributions of these two factors (Eqs. [3] and [4]) to the

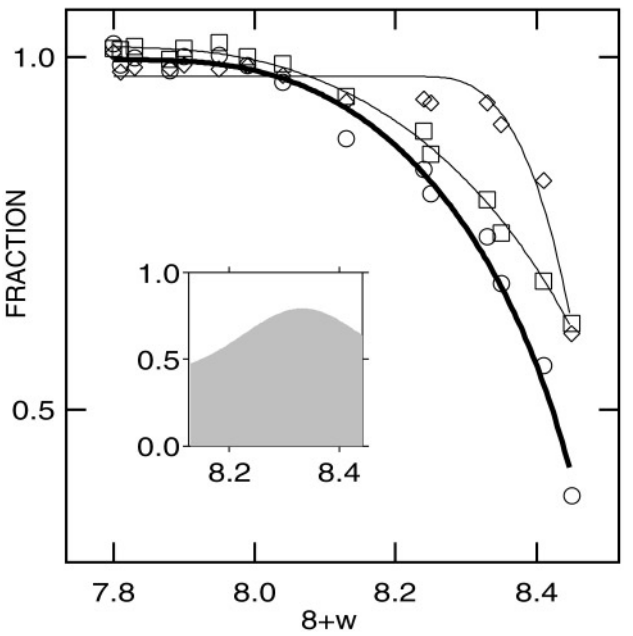

FIG. 8. Fractional average Mössbauer parameters at 296 K (defined in the text): $x_{AF}(\diamond)$, ξ_B^{AF} ($\square$), and $x_{AF}\cdot\xi_B^{AF}$ ($\bigcirc$) as functions of the oxygen content. Inset: Fraction of the overall decrease in B across a sample caused by the weakening of the AF-order (shaded) and by the P centers (unshaded).

overall decrease in the internal field across a sample. The three parameters as functions of w were fitted by a Brillouin-type function, suggesting a resemblance to the well-established magnetic moment vs temperature relationship for cooperative magnetic materials. The common mechanism is that both thermal energy and oxygen loading affect the ordered spin system.

Various kinds of frustration of the coupling forces have been suggested in the literature, often assuming the formation of local ferromagnetic clusters. The disproportionation of Fe^{4+} into Fe^{3+} and Fe^{5+} is suggested in Ref. (28) to align the moments in such clusters. Based on the present room-temperature results, which correspond reasonably to Fe^{4+} as the oxidized state, it seems that the holes in the highly oxidized material have a similar disrupting effect on the moments. In line with Refs. (3–6), it could be argued that these holes are partially present also on the oxygen atoms. An indication in favor of this picture is the single crystal neutron diffraction study (29) of $SrFeO_3$ which locates small ($\sim 0.3\ \mu_B$) moments on the oxygen atoms.

In order to test the assignments for the observed magnetic components, the value of the ordered magnetic moment for each composition ($w > 0$) was estimated as

$$\mu_{AF} = \sum_i \left(\frac{B_{i,w}}{B_{i,sat}} \cdot \frac{I_{i,w}}{100} \cdot 2S_{i,w} \right), \qquad [6]$$

where the intensity of the AF component i is multiplied by the associated spin-only magnetic moment $2S_{i,w}$ (as customary when dealing with Fe). The relative weakening of the internal field at the AF-ordered Fe sites is gauged by the saturation fields $B_{i,sat}$ estimated from the low-temperature data for the practically stoichiometric $w = -0.01$ sample (Table 3). The result is compared in Fig. 9 with the corresponding $\mu_{AF} = 2S$ values obtained by PND in Ref. (8), both curves referring to room-temperature experiments. The outcome can be considered as a match in curve shape between the PND and Mössbauer data. However, the PND magnetic moment falls significantly below the semitheoretical Mössbauer moment, and this may imply that a certain portion of this "theoretical moment" simply does not order on the time and space scales of the PND experiments.

The inset to Fig. 9 illustrates how the individual valence states Fe^{2+}, Fe^{3+}, and Fe^{4+} in $LaBa_2Fe_3O_{8+w}$ contribute to the overall ordered moment as a function of w. When $w = 0$, a small proportion of both Fe^{2+}, and Fe^{4+} could be present simultaneously, as also suggested by electrical conductivity data in Ref. (7). Note that the valence state of Fe^{3+} in Fig. 9 could be further broken down according to CN, corresponding to the model of the random distribution of oxygen vacancies in the disordered cubic perovskite-type structure (Sect. III C1).

The random nature of the distribution of the oxygen vacancies in $LaBa_2Fe_3O_{8+w}$ confirms that there are no

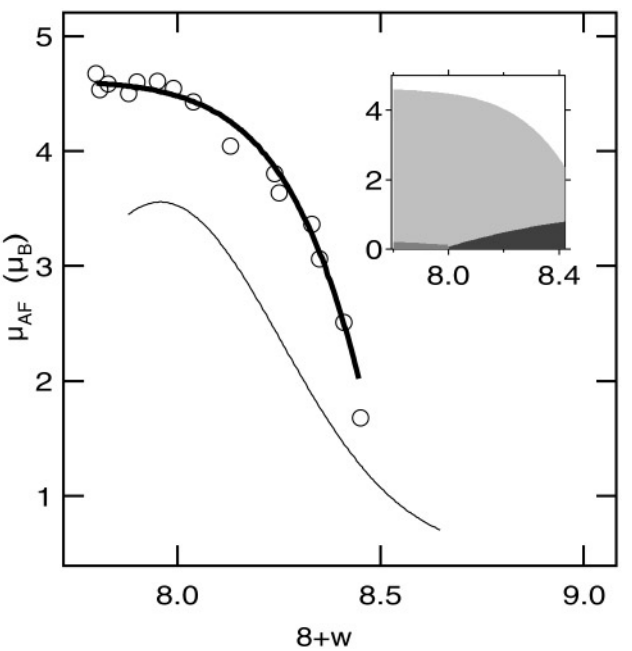

FIG. 9. Ordered magnetic moment $\mu_{AF} = 2S_{AF}$ at 296 K according to PND (thin line, Ref. (8)) and Mössbauer data (according to Eq. [6]) as a function of the oxygen content. Inset: contributions to μ_{AF} according to Mössbauer data for $Fe^{3+}_{S5/2}$ (light shading), Fe^{2+}_{S2} (intermediate shading) and Fe^{4+}_{S2} (heavy shading).

residuals of the triple-perovskite-type ordering, which is otherwise stable when La is replaced by the rare-earth atoms of the group Er–Dy and Y. As these structures contain CN5 and CN6 in the ratio 2:1 ($w = 0$), the random distribution would have been somewhat skewed.

Note added in proof. In $REBa_2Fe_3O_{8+w}$ phases with RE = Nd, Sm, and Gd, the authors have been able to distinguish two components originating from divalent iron, assigned $^{CN4}_{AF}Fe^{2+}_{S2}$ and $^{CN3}_{AF}Fe^{2+}_{S2}$. With this new knowledge, it has been possible to obtain agreement between analytical and Mössbauer iron valence states. The origin of these two components will be discussed in a forthcoming paper.

ACKNOWLEDGMENTS

Mr. J. Miettinen is acknowledged for his assistance with Mössbauer measurements.

REFERENCES

1. I. Morgenstern, *Z. Phys. B*: *Condens. Matter* **70,** 229 (1988).
2. J. Kitaoka, K. Ishida, S. Hiramatsu, and K. Asayama, *J. Phys. Soc. Jpn.* **57,** 734 (1988).
3. A. Aharony, R. J. Birgenau, A. Conigli, M. A. Kastner, and H. E. Stanley, *Phys. Rev. Lett.* **60,** 1330 (1988).
4. V. J. Emery and G. Reiter, *Phys. Rev. B*: *Condens. Matter* **38,** 4547 (1988).
5. M. Kohomoto and J. Friedel, *Phys. Rev. B*: *Condens. Matter* **38,** 7054 (1988).
6. Y. Guo, J.-M. Langlois, and W. A. Goddard, *Science* **239,** 896 (1988).
7. P. Karen and T. Norby, to be published.
8. P. Karen, A. Kjekshus, Q. Huang, J. W. Lynn, N. Rosov, I. Natali Sora, V. L. Karen, A. D. Mighell, and A. Santoro, *J. Solid State Chem.* **136,** 21 (1998).
9. Q. Huang, P. Karen, V. L. Karen, A. Kjekshus, J. W. Lynn, A. D. Mighell, N. Rosov, and A. Santoro, *Phys. Rev. B*: *Condens. Matter* **45,** 9611 (1992).
10. J. Li and J. Jing, *Hyperfine Interact.* **69,** 569 (1991).
11. M. Parras, M. Vallet-Regí, J. M. González-Calbet, M. Alario-Franco, and J. C. Grenier, *J. Solid State Chem.* **74,** 110 (1988).
12. T. C. Gibb and M. Matsuo, *J. Solid State Chem.* **81,** 83 (1989).
13. J. M. Gonzáles-Calbet, M. Parras, M. Vallet-Regí, and J. C. Grenier, *J. Solid State Chem.* **92,** 110 (1991).
14. A. Elzubair and M. El Massalami, *Physica B* (*Amsterdam*) **225,** 53 (1996).
15. P. Karen and A. Kjekshus, *J. Am. Ceram. Soc.* **77,** 547 (1994).
16. I. Barin and O. Knacke, "Thermochemical Properties of Inorganic Substances," pp. 316, 584. Springer, Berlin, 1973.
17. I. Barin, O. Knacke, and O. Kubashevski, "Thermochemical Properties of Inorganic Substances, Supplement," p. 295. Springer, Berlin, 1977.
18. P. E. Werner, "The Computer Programme SCANPI 9." Institute of Inorganic Chemistry, University of Stockholm, Sweden 1992.
19. E. García-González, M. Parras, J. M. González-Calbet, and M. Vallet-Regí, *J. Solid State Chem.* **105,** 363 (1993).
20. R. W. Grant, *in* "Mössbauer Spectroscopy," (U. Gonser. Ed.), p. 1069, Springer, Berlin, 1975.
21. N. N. Greenwood and T. C. Gibb, "Mössbauer Spectroscopy," p. 91, Chapman and Hall, London, 1971.
22. P. Gütlich, *in* "Mössbauer Spectroscopy," (U. Gonser. Ed.), p. 82. Springer, Berlin, 1975.
23. M. Takano, N. Nakanishi, Y. Takeda, S. Naka, and T. Takada, *Mater. Res. Bull.* **12,** 923 (1977).
24. Y. Takeda, S. Naka, M. Takano, T. Shinjo, T. Takada, and M. Shimada, *Mater. Res. Bull.* **13,** 61 (1978).
25. M. Takano, J. Kawachi, N. Nakanishi, and Y. Takeda, *J. Solid State Chem.* **39,** 75 (1981).
26. S. E. Dann, D. B. Currie, M. T. Weller, M. F. Thomas, and A. D. Al-Rawwas, *J. Solid State Chem*, **109,** 134 (1994).
27. P. Adler, *J. Solid State Chem.* **130,** 129 (1997).
28. P. D. Battle, T. C. Gibb, P. Lightfoot, and M. Matsuo, *J. Solid State Chem.* **85,** 38 (1990).
29. H. Oda, Y. Yamaguchi, H. Takei, and H. Watanabe, *J. Phys. Soc. Jpn* **42,** 101 (1977).